# Perturbation model for optical modes in deformed disks

Tianpeng Jiang and Yang Xiang*
*Department of Mathematics, The Hong Kong University of Science and Technology, Clear Water Bay, Kowloon, Hong Kong*

(Received 24 March 2018; published 25 February 2019)

We present a perturbation approach to calculate the optical modes in arbitrary weakly deformed disks. By introducing a small perturbation parameter into the mode equation and interface conditions, the original problem is decomposed into different orders of perturbation problems. In this paper, we focus on the linear perturbation method, which is able to provide good approximations to solutions for arbitrary weakly deformed disks. Our linear perturbation method is able to explain the mode-splitting phenomena of the clockwise and counterclockwise degeneracy. We apply our perturbation method to limaçon and spiral cavities, and the perturbation results agree well with numerical results of the full problem.

DOI: 10.1103/PhysRevA.99.023847

## I. INTRODUCTION

Dielectric microdisk cavities [1] are of great use in controlling light-matter interactions in photonic technology such as microlasers [2], optical filters [3], nanoparticle sensors [4,5], and optical gyroscopes [6]. The optical modes formed in uniform disk are called whispering-gallery modes (WGMs) [7]. Due to total internal reflection at the edge of the disk, WGMs possess long photon lifetimes and hence high-quality factors. However, because uniform disks have has rotational symmetry, WGMs perform isotropic emission along all directions of the cavity rim, which makes WGMs-based devices energy-inefficient. In order to inherit high-quality-factor merit of the uniform disk and to possess a directional emission pattern simultaneously, one of the ideas is to break disk symmetry by introducing weak deformation into the cavity shape, such as spiral [8–11], limaçon [12–17], ellipse [18–20], near disk [21–23], and annular [24]. Directly constructing an ideal deformed disk shape for a designed mode pattern is very challenging. In order to achieve this goal, it is necessary first to establish a theory that is able to calculate optical modes in an arbitrary weakly deformed disk, and second to figure out the cavity shape to achieve a given mode pattern (the inverse problem).

In deformed cavities, although numerical methods can be applied to solve the optical modes, it is difficult to analyze with numerical solutions the inverse problem [25] and other interesting phenomena such as wave chaos [26–29] and non-Hermitian physics [30–32], where analytical solutions are needed. A method based on perturbation theory for weakly deformed mirror-symmetric disks was developed by Dubertrand *et al.* by introducing an artificially constructed perturbation series [33]. Their perturbation method was further applied to cut-disk cavities [33], limaçon cavities [16], and double-cosine and triple-cosine polar cavities [34]. This method is limited by presuming mirror-reflection symmetry of a deformed disk and therefore cannot be applied to arbitrary weakly deformed disks. To solve this problem, Kullig *et al.* modified the perturbation series and extended the method from symmetric to asymmetric cavities and further applied it to spiral cavities and studied its mode chirality [10]. However, these methods are based on perturbation series of functions with a prescribed form, which are not necessarily the accurate solutions of the perturbation equations for arbitrary weakly deformed disks.

In this paper, we present an approximation approach based on perturbation theory to optical modes in weakly deformed disks. Our method uses rigorous perturbation expansions of the equation and boundary conditions without prescribing the form of solutions; they are rigorously solved from the perturbation problems. Additionally, our method provides a framework for obtaining perturbation solutions up to any order. In this paper, we focus on solutions of linear perturbation. Linear perturbations in general have the advantage of a relatively simple form in solutions compared with higher order when analyzing the inverse problem and the wave chaos phenomenon.

We apply our perturbation method to limaçon and spiral cavities, and the perturbation results agree well with numerical results of the full problem. Compared with the available perturbation methods in literature which use up to second-order perturbation terms [10,33], our linear perturbation method provides better approximations to the optical mode patterns for arbitrary weakly deformed disks. For the resonance, the results obtained using our linear perturbation method are almost the same as those of the available first-order perturbations in the literature. Moreover, our linear perturbation result is able to explain the mode-splitting phenomena of the clockwise and counterclockwise degeneracy. Our perturbation method accurately demonstrates mode patterns at quasidegenerate points in spiral cavities, where the perturbation methods in literature fail [10]. Even if deformations of the disk become relatively large where the method in literature breaks down [16], our perturbation method is still able to provide reasonably good approximations to the mode patterns.

The rest of the paper is organized as follows. We first briefly present the mathematical description of the problem

*maxiang@ust.hk

 

and the results of WGMs in Sec. II. Then we introduce our perturbation treatment to the problem and discuss the mode-splitting phenomenon in Sec. III. Finally, we apply our perturbation method to limaçon and spiral cavities in Sec. IV.

## II. THE WHISPERING-GALLERY MODES

Optical devices are usually fabricated on a material layer of very thin thickness compared with in-plane dimensions. Therefore, the problem is naturally reduced to two dimensions, where the refractive index inside cavity should be replaced by an effective refractive index in real applications. Mathematical description of optical modes in arbitrary cavities consists of three parts [35]: the mode equation, interface conditions, and boundary condition.

The stationary electric and magnetic field pattern is governed by the mode equation, which is derived from Maxwell's equation and finally reduced to a Helmholtz-type eigenequation:

$$\nabla^2\psi + (nk)^2\psi = 0, \tag{1}$$

where $n$ is refractive index being piecewise constant, i.e., $n_1$ and $n_2$ for inside and outside of the cavity domain $\Omega$ (further denote $\partial\Omega^+$ and $\partial\Omega^-$ as cavity rim inside and outside, respectively). The quasieigenvalue of the mode equation is a free-space wave number $k$ (which also stands for mode resonance because $k = \omega/c$, where $c$ is the light speed constant). The quasieigenfunction of the mode equation is the mode pattern $\psi(\rho, \phi)$, representing either $E_z$ for the transverse magnetic (TM) mode or $B_z$ for the transverse electric (TE) mode. Interface conditions of electromagnetic field are given by the following continuity relations for the TM mode:

$$\psi|_{\partial\Omega^+} = \psi|_{\partial\Omega^-}, \quad \left.\frac{\partial\psi}{\partial\phi}\right|_{\partial\Omega^+} = \left.\frac{\partial\psi}{\partial\phi}\right|_{\partial\Omega^-}, \quad \left.\frac{\partial\psi}{\partial\rho}\right|_{\partial\Omega^+} = \left.\frac{\partial\psi}{\partial\rho}\right|_{\partial\Omega^-}, \tag{2}$$

and similarly for the TE mode.

Moreover, the mode pattern must satisfy Sommerfeld's radiation condition [36], which is the boundary condition preventing waves coming from infinity.

A uniform disk with radius of $\rho_0$ is a special case in which its optical modes (WGMs) can be directly calculated using the method of separation of variables [7]. The obtained WGMs consist of infinitely many discretized resonances $k_{m,j}$, denoted by mode index $(m, j)$ where $m$ $(m = 1, 2, \ldots)$ is the azimuthal order and $j$ $(j = 1, 2, \ldots)$ is the radial order. Because a uniform disk has rotational symmetry, each $k_{m,j}$ associates with mode patterns of twofold degeneracy, the clockwise mode (CW) and counterclockwise mode (CCW):

$$\text{CW:} \quad \varphi_{m,j}(\rho, \phi) = N_{m,j}R_m(k_{m,j}\rho)\frac{e^{im\phi}}{\sqrt{2\pi}}, \tag{3a}$$

$$\text{CCW:} \quad \varphi_{-m,j}(\rho, \phi) = N_{m,j}R_m(k_{m,j}\rho)\frac{e^{-im\phi}}{\sqrt{2\pi}}, \tag{3b}$$

where $R_l(k_{m,j}\rho)$ is the radial function defined as

$$R_l(k_{m,j}\rho) = \begin{cases} \mathcal{J}_l(n_1k_{m,j}\rho)/\mathcal{J}_l(n_1k_{m,j}\rho_0) & \text{if } \rho \leqslant \rho_0 \\ \mathcal{H}_l(n_2k_{m,j}\rho)/\mathcal{H}_l(n_2k_{m,j}\rho_0) & \text{if } \rho > \rho_0 \end{cases}. \tag{4}$$

and $\mathcal{H}_l$, $\mathcal{J}_l$ are the $l$th-order of Bessel function of the first kind and Hankel function of the first kind, respectively. The constants $N_{m,j}$ and $\sqrt{2\pi}$ are introduced to normalize $R_m(k_{m,j}\rho)$ and $e^{\pm im\phi}$ such that the approximate orthogonality in the radial and azimuthal directions can be obtained:

$$N_{m,j}^2\int_0^{+\infty} n^2R_m^*(k_{m,i}\rho)R_m(k_{m,j}\rho)\rho\,d\rho = \delta_{i,j}, \tag{5a}$$

$$\frac{1}{2\pi}\int_{-\pi}^{\pi} e^{-i(l-m)\phi}\,d\phi = \delta_{l,m}. \tag{5b}$$

The orthogonality above can be combined to give the orthogonal relation of mode patterns:

$$\int_{\mathbb{R}^2} n^2\varphi_{l,i}^*\varphi_{m,j}\,ds = \delta_{l,m}\delta_{i,j}. \tag{6}$$

The orthogonal relations in Eqs. (5a) and (6) are approximate conditions. Because the interface conditions and the boundary conditions cannot strictly bound electromagnetic waves, WGMs are intrinsically energy-dissipating. Therefore, each $k_{m,j}$ is a complex number with the real and imaginary parts denoting mode frequency and decay rate, respectively. The mode quality factor can be expressed as $Q = |\mathrm{Re}(k_{m,j})/2\mathrm{Im}(k_{m,j})|$. However, WGMs could still be approximated as orthogonal due to $|\mathrm{Im}(k_{m,j})| \ll |\mathrm{Re}(k_{m,j})|$ which states that mode patterns are quickly built up before starting to dissipate. Moreover, the orthogonal relation Eq. (6) could be interpreted as no coupling between different optical modes.

## III. PERTURBATION TREATMENT

### A. Perturbation expansions

Although optical modes in uniform disk cavity can be treated directly, many photonic devices utilize varieties of deformed cavities. In our perturbation approach, we express an arbitrary weakly deformed disk shape in polar coordinates as

$$G(\phi) = \rho_0 + \epsilon f(\phi), \tag{7}$$

where $\epsilon$ is a dimensionless perturbation parameter and $f(\phi)$ denotes deformation.

For a deformed disk, the mode equation (1) and the interface conditions (2) are still valid but in the deformed cavity domain. The mode pattern and resonance can be written in power expansions of $\epsilon$:

$$\psi = \psi^{(0)} + \epsilon\psi^{(1)} + \epsilon^2\psi^{(2)} + \cdots = \sum_{i=0}^{\infty}\epsilon^i\psi^{(i)}, \tag{8}$$

$$k = k^{(0)} + \epsilon k^{(1)} + \epsilon^2 k^{(2)} + \cdots = \sum_{i=0}^{\infty}\epsilon^i k^{(i)}. \tag{9}$$

Substituting Eqs. (8) and (9) into the mode equation (1), we can collect perturbation equations in orders of $\epsilon$:

$$\sum_{l=0}^{\infty}\epsilon^l\left[\nabla^2\psi^{(l)}+n^2\sum_{i=0}^{l}\sum_{j=0}^{i}k^{(j)}k^{(i-j)}\psi^{(l-i)}\right]=0. \quad (10)$$

By performing the Taylor expansion at $\rho=\rho_0$ and replacing $\psi$ with the power expansion in Eq. (8), we get the continuity relations that are equivalent to those in Eq. (2) and hold at $\rho=\rho_0$ instead of $\rho=G(\phi)$ (i.e., $\partial\Omega$), with the following expansions:

$$\psi|_{\rho=G(\phi)}=\sum_{l=0}^{\infty}\epsilon^l\sum_{i=0}^{l}\frac{[f(\phi)]^i}{i!}\frac{\partial^i\psi^{(l-i)}}{\partial\rho^i}\bigg|_{\rho=\rho_0}, \quad (11a)$$

$$\frac{\partial\psi}{\partial\phi}\bigg|_{\rho=G(\phi)}=\sum_{l=0}^{\infty}\epsilon^l\sum_{i=0}^{l}\frac{[f(\phi)]^i}{i!}\frac{\partial^{i+1}\psi^{(l-i)}}{\partial\phi\partial\rho^i}\bigg|_{\rho=\rho_0}, \quad (11b)$$

$$\frac{\partial\psi}{\partial\rho}\bigg|_{\rho=G(\phi)}=\sum_{l=0}^{\infty}\epsilon^l\sum_{i=0}^{l}\frac{[f(\phi)]^i}{i!}\frac{\partial^{i+1}\psi^{(l-i)}}{\partial\rho^{i+1}}\bigg|_{\rho=\rho_0}. \quad (11c)$$

Collecting perturbation equations and interface conditions of the same order leads to series perturbation problems in orders of $\epsilon$.

### B. Leading-order perturbation problem

The leading-order problem reproduces the unperturbed problem, with the governing equation:

$$\nabla^2\psi^{(0)}+(nk^{(0)})^2\psi^{(0)}=0 \quad (12)$$

and interface conditions:

$$\psi^{(0)}|_{\rho=\rho_0^+}^{\rho=\rho_0^-}=0,\quad \frac{\partial\psi^{(0)}}{\partial\phi}\bigg|_{\rho=\rho_0^+}^{\rho=\rho_0^-}=0,\quad \frac{\partial\psi^{(0)}}{\partial\rho}\bigg|_{\rho=\rho_0^+}^{\rho=\rho_0^-}=0. \quad (13)$$

Therefore, $k^{(0)}$ should be the same as the unperturbed resonance, i.e., $k\to k^{(0)}=k^{(0)}_{m,j}$ as $\epsilon\to 0$, for any mode $(m,j)$.

On the other hand, the mode patterns are not necessarily the same as the unperturbed ones due to mode degeneracy. Equation (8) indicates that $\psi\to\psi^{(0)}$ as $\epsilon\to 0$, each $k^{(0)}_{m,j}$ associates with CW-CCW degeneracy, and any linear combination of them is an eigenfunction associated with the same resonance. This means that with all information of the leading-order problem, we cannot determine, as $\epsilon\to 0$, what combination of $\varphi_{m,j}$ and $\varphi_{-m,j}$ the perturbed mode pattern should converge to. Therefore, we can only assume the leading of $\psi$ takes the form

$$\psi^{(0)}_{m,j}=c_1\varphi_{m,j}+c_2\varphi_{-m,j}, \quad (14)$$

where the constant coefficients $c_1$ and $c_2$ are to be determined.

### C. First-order perturbation problem

The governing equation of the first-order problem is an inhomogeneous Helmholtz equation driven by leading order:

$$\nabla^2\psi^{(1)}_{m,j}+(nk^{(0)}_{m,j})^2\psi^{(1)}_{m,j}=-2n^2k^{(0)}_{m,j}k^{(1)}_{m,j}\psi^{(0)}_{m,j}. \quad (15)$$

Corresponding interface conditions can be simplified as

$$\psi^{(1)}_{m,j}\Big|_{\rho=\rho_0^+}^{\rho=\rho_0^-}=0,\quad \frac{\partial\psi^{(1)}_{m,j}}{\partial\phi}\bigg|_{\rho=\rho_0^+}^{\rho=\rho^-}=0, \quad (16a)$$

$$\frac{\partial\psi^{(1)}_{m,j}}{\partial\rho}\bigg|_{\rho=\rho_0^+}^{\rho=\rho_0^-}=-f(\phi)\frac{\partial^2\psi^{(0)}_{m,j}}{\partial\rho^2}\bigg|_{\rho=\rho_0^+}^{\rho=\rho_0^-}. \quad (16b)$$

The first-order perturbation problem can be solved with separation of variables: $\psi^{(1)}_{m,j}=\sum_l g_l(\rho)e^{il\phi}/\sqrt{2\pi}$. To simplify the results, the following notions will be used:

$$W_l(\rho)=\frac{\mathcal{J}_l\left(n_1k^{(0)}_{m,j}\rho\right)}{\mathcal{J}_l\left(n_1k^{(0)}_{m,j}\rho_0\right)}-\frac{\mathcal{H}_l\left(n_2k^{(0)}_{m,j}\rho\right)}{\mathcal{H}_l\left(n_2k^{(0)}_{m,j}\rho_0\right)}, \quad (17a)$$

$$\cos(2\theta_m)=\frac{\int_{-\pi}^{\pi}f(\phi)\cos(2m\phi)\,d\phi}{\left|\int_{-\pi}^{\pi}f(\phi)e^{i\cdot2m\phi}\,d\phi\right|}, \quad (17b)$$

$$\sin(2\theta_m)=\frac{\int_{-\pi}^{\pi}f(\phi)\sin(2m\phi)\,d\phi}{\left|\int_{-\pi}^{\pi}f(\phi)e^{i\cdot2m\phi}\,d\phi\right|}. \quad (17c)$$

In fact, integrating $g_{\pm m}(\rho)$ with the complex conjugate of $\rho R_m(k^{(0)}_{m,j}\rho)$ and substituting the orthogonal relation (5a) could give an algebraic eigenequation:

$$\begin{pmatrix}f_0 & f_{2m}\\ f_{-2m} & f_0\end{pmatrix}\begin{pmatrix}c_1\\ c_2\end{pmatrix}=\frac{2k^{(0)}_{m,j}k^{(1)}_{m,j}}{\rho_0N^2_{m,j}W''_m(\rho_0)}\begin{pmatrix}c_1\\ c_2\end{pmatrix}, \quad (18)$$

where matrix entries are Fourier coefficients of $f(\phi)$, i.e., $f_k=\frac{1}{2\pi}\int_{-\pi}^{\pi}f(\phi)e^{-ik\phi}\,d\phi$. The eigensolutions are the first-order resonance $k^{(1)}_{m,j}$ and the coefficients $c_1$ and $c_2$ in Eq. (14):

$$k^{(1)}_{m,j,s}=k^{(1)}_{m,j,\pm}=\frac{\rho_0N^2_{m,j}W''_m(\rho_0)}{2k^{(0)}_{m,j}}(f_0\pm\sqrt{f_{2m}f_{-2m}}), \quad (19)$$

$$(c_{1,s},c_{2,s})=(c_{1,\pm},c_{2,\pm})=(e^{-i\theta_m},\pm e^{i\theta_m})/\sqrt{2\pi}, \quad (20)$$

where another mode index $s$ (either $+$ or $-$) is introduced to denote splitting of mode degeneracy.

Integrating Eq. (7) over one period leads to $2\pi(\rho_0+\epsilon f_0)=\int_{-\pi}^{\pi}G(\phi)\,d\phi$, which means that $\epsilon f_0$ is a correction of cavity radius and can always be set as zero if an unperturbed cavity radius is properly chosen. The second term $\sqrt{f_{2m}f_{-2m}}$ in Eq. (19) gives an estimate of resonance splitting. Note that the splitting term might be zero in special cases, where higher-order perturbations are needed to further separate the degeneracy.

Corresponding eigenvectors given in Eq. (20) lead to the following leading-order mode patterns with Eq. (14):

$$\psi^{(0)}_{m,j,+}=N_{m,j}R_m\left(k^{(0)}_{m,j}\rho\right)\cos(m\phi-\theta_m)/\sqrt{\pi}, \quad (21a)$$

$$\psi^{(0)}_{m,j,-}=N_{m,j}R_m\left(k^{(0)}_{m,j}\rho\right)\sin(m\phi-\theta_m)/\sqrt{\pi}. \quad (21b)$$

From Eq. (20), it is easy to see both $\psi^{(0)}_{m,j,+}$ and $\psi^{(0)}_{m,j,-}$ are made up half from CW and half from CCW. The phase differences between CW and CCW are $2\theta_m$ and $(2\theta_m+\pi)$ for $s=+$ and $-$, respectively. The leading-order mode patterns $\psi^{(0)}_{m,j,\pm}$ are results of disk symmetry breaking and associated with cavity deformation through the parameter $\theta_m$, which

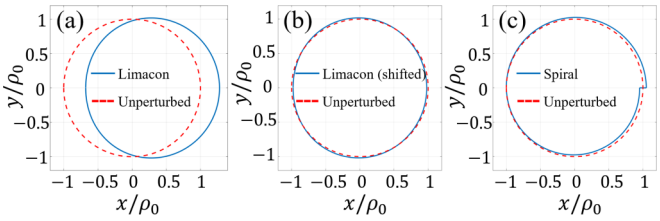


FIG. 1. Deformed cavity shapes: (a) limaçon without shifting, (b) limaçon with shifting, (c) spiral shape; the red dash lines are unperturbed disks with radius of $\rho_0$.

depends on the detailed profile of the deformation $f(\phi)$ and is independent of the perturbation amplitude.

The first-order perturbation problem [Eqs. (15) and (16)] also give the first-order correction of the mode pattern as

$$\psi^{(1)}_{m,j,s} = -\sum_{l\neq\pm m} \frac{N_{m,j}W''_m(\rho_0)}{\pi^{3/2}W''_l(\rho_0)}\left[\alpha_{l,s}R_l\left(k^{(0)}_{m,j}\rho\right)\cos(l\phi)\right.$$
$$\left.+\,\beta_{l,s}R_l\left(k^{(0)}_{m,j}\rho\right)\sin(l\phi)\right], \tag{22}$$

in which $\alpha_{l,s}$ and $\beta_{l,s}$ are defined as

$$\alpha_{l,+} = \int_{-\pi}^{\pi} f(\xi)\cos(l\xi)\cos(m\xi-\theta_m)\,d\xi, \tag{23a}$$
$$\beta_{l,+} = \int_{-\pi}^{\pi} f(\xi)\sin(l\xi)\cos(m\xi-\theta_m)\,d\xi, \tag{23b}$$
$$\alpha_{l,-} = \int_{-\pi}^{\pi} f(\xi)\cos(l\xi)\sin(m\xi-\theta_m)\,d\xi, \tag{23c}$$
$$\beta_{l,-} = \int_{-\pi}^{\pi} f(\xi)\sin(l\xi)\sin(m\xi-\theta_m)\,d\xi. \tag{23d}$$

### D. Higher-order perturbation problem

Higher-order perturbation problems are also constructed under our perturbation framework. In fact, by collecting the same order term $O(\epsilon^l)$ $(l = 2, 3, 4, \ldots)$ in Eq. (10) and Eq. (11), the governing equation and interface conditions of higher order could be obtained, respectively. However, in this paper the mode resonance and patterns are extended to first order, and the error is estimated within $O(\epsilon^2)$.

## IV. APPLICATIONS TO LIMAÇON AND SPIRAL CAVITY

We apply our perturbation method to two generics of weakly deformed disks, limaçon and spiral; see Fig. 1. To validate our perturbation method, we compare our perturbation results with numerically exact results calculated using the finite element method (FEM). For purposes of direct comparisons with available results in the literature [10,16], we set the refractive index to $n_1 = 2$ and $n_2 = 1$ for both limaçon and spiral cavities.

### A. Application to limaçon

The limaçon shape, shown in Fig. 1(a), is defined as $G(\phi) = r(1 + \epsilon\cos\phi)$, where $\epsilon$ is the deformation parameter. By shifting the reference coordinate, improvement of the perturbation approximation has been demonstrated [16]. Here

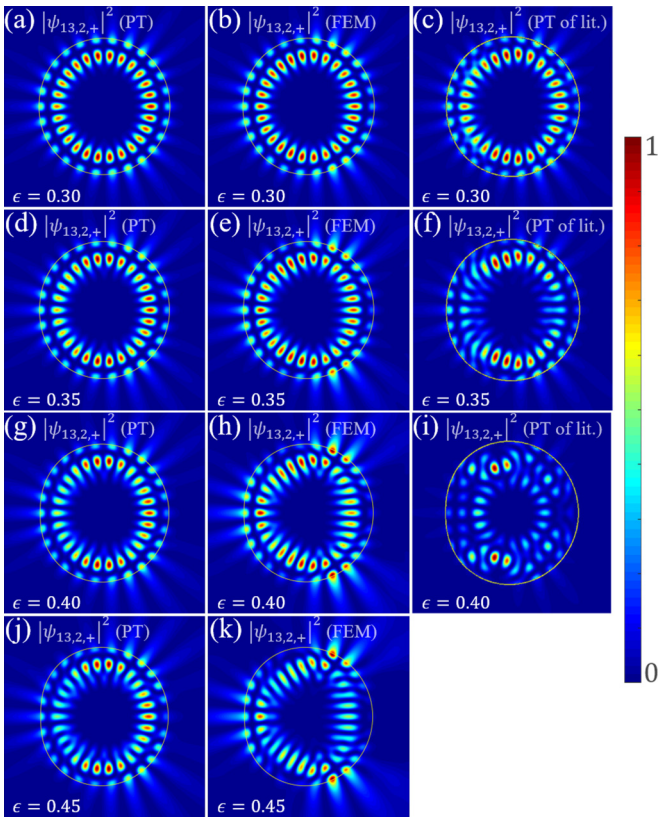


FIG. 2. Limaçon cavity mode pattern $|\psi_{13,2,+}(\rho,\phi)|^2$ with increasing deformation parameter: (a–c) $\epsilon = 0.3$, (d–f) $\epsilon = 0.35$, (g–i) $\epsilon = 0.4$, (j, k) $\epsilon = 0.45$. Panels (a), (d), (g), and (j) are our perturbation (PT) results; (b), (e), (h), and (k) are the full numerical results calculated with the finite element method (FEM); (c), (f), and (i) are results of the existing perturbation method (in Fig. 10 of Ref. [16]).

we adopt the reference coordinate shifting [see Fig. 1(b)] and define the unperturbed disk radius $\rho_0$ in such a way that the radius correction $\epsilon f_0$ is zero. Due to the even symmetry of the limaçon cavity, the phase difference $\theta_m = 0$ and the mode pattern are either a cosine form $(s = +)$ or sine form $(s = -)$ according to Eqs. (21) and (22). This form recovers the prescribed sine and cosine expansions used in the existing perturbation methods in Refs. [16,33] that work for symmetric cavities.

Figure 2 shows the obtained results of mode pattern $|\psi|^2$ using our perturbation method, and comparisons with the full numerical results and the results of the existing perturbation theory reported in Ref. [16] (in their Fig. 10), under different values of perturbation amplitude $\epsilon$. The mode patterns are compared under the same mode index, i.e., $(13, 2, +)$, and the figures in the same row are under the same values of the perturbation amplitude. It can be seen from Fig. 2 that our perturbation method gives better approximations than the method in Ref. [16] as the perturbation amplitude increases. When $\epsilon = 0.40$, the mode pattern obtained by the existing perturbation method deviates significantly from the exact result, whereas the result of our method is still quite good. In the last panel of Fig. 2, comparison of our perturbation result with the

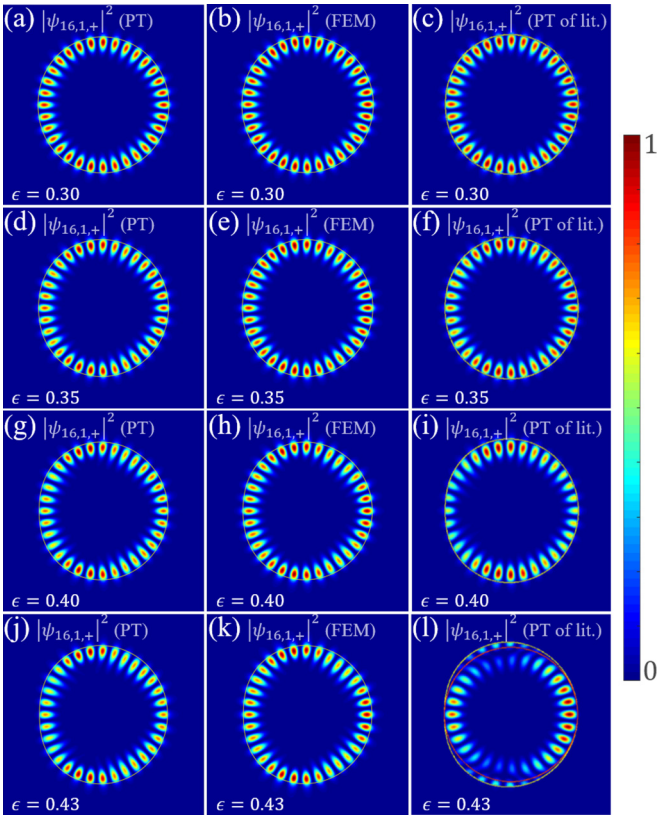


FIG. 3. Limaçon cavity mode pattern $|\psi_{16,1,+}(\rho,\phi)|^2$ with increasing deformation parameter: (a–c) $\epsilon = 0.3$, (d–f) $\epsilon = 0.35$, (g–i) $\epsilon = 0.4$, (j–l) $\epsilon = 0.43$. Panels (a), (d), (g), and (j) are our perturbation (PT) results; (b), (e), (h), and (k) are full numerical results calculated with FEM; (c), (f), (i), and (l) are results of existing perturbation method (in Fig. 8 of Ref. [16])

exact one is shown for even larger perturbation amplitude, $\epsilon = 0.45$, where our perturbation method still works reasonably.

We also calculate the mode pattern $|\psi|^2$ for mode $(16, 1, +)$ using our perturbation method and make comparisons with the full numerical results and the results of the existing perturbation method reported in Ref. [16] (in their Fig. 8), under the same values of the perturbation amplitude. The comparisons are shown in Fig. 3. The same conclusions can be drawn as in the comparisons for the mode $(13, 2, +)$ discussed above. Our perturbation method gives better approximations to mode patterns than the method in Ref. [16] as the perturbation amplitude increases. When $\epsilon = 0.43$, the mode pattern obtained by the existing perturbation method deviates significantly from numerical result, whereas our perturbation results are well matched with numerical result.

We calculate the dimensionless resonances $k\rho_0$ for mode $(13, 2, +)$ using our perturbation method and compare with the full numerical results and the results of perturbation theories in Ref. [16]; see Fig. 4. The real part of the resonance calculated by our perturbation method is very accurate for perturbation amplitude $\epsilon \leqslant 0.5$, with relative error less than 0.3%; see Fig. 4(a) (note the very fine scale in the vertical axis). The calculated imaginary part of the resonance also agrees well with the numerical result for $\epsilon \leqslant 0.25$; see

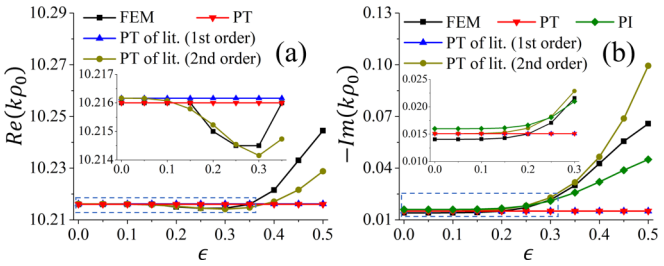


FIG. 4. Dimensionless resonance of mode $(13, 2, +)$ of the limaçon cavity: (a) real part and (b) imaginary part; comparisons are shown between our perturbation results (PT, red), FEM results (black), first-order perturbation (blue), second-order perturbation (yellow) of Ref. [16], and Poynting vector integration (PI, green). The insertion is a finer plot of the region marked by the dash box in each image. Here $\rho_0$ is the radius of the unperturbed disk.

Fig. 4(b). When $\epsilon$ becomes larger, the error of the calculated imaginary part increases rapidly because the imaginary part is highly sensitive to the cavity deformation. For both real and imaginary parts of the resonance, our results and the first-order perturbation results of Ref. [16] are almost the same in these cases. Their second-order perturbation results do show improved accuracy, which are still quite good up to around $\epsilon = 0.4$ for the imaginary part. The approximations using our perturbation framework are also expected to be improved when second-order or even higher-order nonlinear perturbation terms are included, which will be done in the future work.

On the other hand, we improve our calculation of the imaginary part of resonance by integration of the Poynting vector [37]. The Poynting vector stands for the outward energy flux,

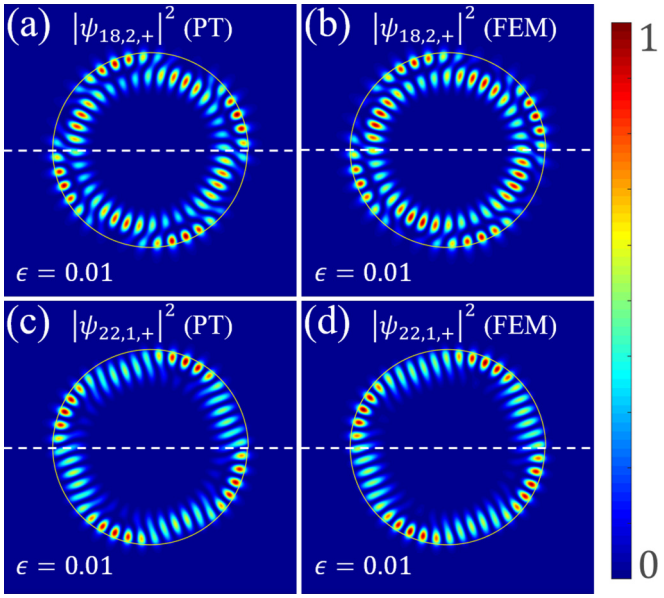


FIG. 5. Spiral cavity mode pattern $|\psi(\rho,\phi)|^2$ at the quasidegenerate points, i.e., (18, 2) and (22, 1). The mode patterns on the left panel are our perturbation (PT) results, and those on the right panel are numerical results calculated with FEM. The dashed lines are the $x$ axis.

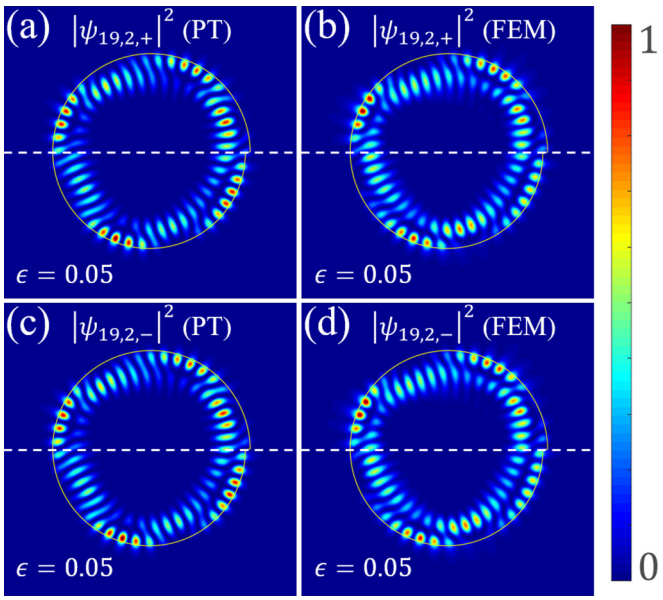


FIG. 6. Spiral cavity mode pattern $|\psi(\rho,\phi)|^2$ of CW-CCW degeneracy splitting at $(19, 2)$. The mode patterns on the left panel are our perturbation (PT) results, and those on the right panel are numerical results calculated by FEM. The dashed lines are the $x$ axis.

and therefore the integration characterizes the total energy decay rate [35], which is the imaginary part of resonance. The imaginary part of resonance can be calculated as

$$\mathrm{Im}(k) = -\frac{i}{4\mathrm{Re}(k)} \frac{\oint_{\partial\Omega}\left(\psi \frac{\partial\psi^*}{\partial r} - \psi^* \frac{\partial\psi}{\partial r}\right) dl}{\int_\Omega n^2 |\psi|^2 \, dS}, \tag{24}$$

where $\Omega$ stands for the cavity domain and $\psi$ is the mode distribution. We use our first-order perturbation approximation $\psi^{(0)}_{13,2} + \epsilon\psi^{(1)}_{13,2}$ as the total mode distribution in Eq. (24) and calculate the imaginary part of resonance, shown as the green line in Fig. 4(b). It can be seen that even though we use mode distribution of linear perturbation in the calculation, the calculated imaginary part of resonance is much improved by integration of the Poynting vector. This is due to the nonlinearity introduced by the integration of the Poynting vector.

### B. Application to spiral

Next, we apply our perturbation method to a spiral cavity: a generic version of asymmetric cavities. The spiral shape [see Fig. 1(c)] is defined as $G(\phi) = \rho_0(1 + \epsilon\phi/2\pi), -\pi \leqslant \phi < \pi$, where $\epsilon$ is the deformation parameter.

We first perform calculations for modes of $(18, 2)$ and $(22, 1)$, where the unperturbed resonance is almost the same: $k^{(0)}_{18,2}\rho_0 = 13.135 - 0.00121i$ and $k^{(0)}_{22,1}\rho_0 = 13.143 - 0.00000074i$, which is the case of quasidegeneracy. The perturbation method presented in Ref. [10] failed at quasidegeneracy due to the closeness of resonances. On the other hand, our method is able to accurately give the mode patterns at the quasidegeneracy for small perturbations with $\epsilon = 0.01$; see the mode patterns shown in Fig. 5.

Other than quasidegenerate points, our perturbation method works well even at a relatively large deformation. We fix the spiral cavity with $\epsilon = 0.05$ and apply our perturbation method to mode $(19, 2)$ to study CW-CCW splitting. Shown in Fig. 6, our perturbation method successfully gives splitting mode patterns $|\psi_{19,2,\pm}|^2$. The mode patterns $|\psi_{19,2,\pm}|^2$ have similar period-four structures (so-called quasiscar [11]) with some difference in rotation with respect to the disk center, which demonstrates the effect of $\theta_m$. After the CW and CCW splitting is determined, the mode chirality [10,38–41] and other interesting properties can be further quantified and analyzed.

## V. CONCLUSIONS

In this paper, we present a perturbation method to describe optical modes in arbitrary weakly deformed disks. In the perturbation treatment, we introduce a small parameter $\epsilon$ into the deformed disk shape and represent the mode pattern and resonance in power expansions of $\epsilon$. This leads to decomposition of the mode equation and interface conditions into a series of perturbation problems in orders of $\epsilon$. We focus on linear perturbations, which are able to provide good approximations to solutions for arbitrary weakly deformed disks. Our linear perturbation method is able to explain the mode-splitting phenomena of the clockwise and counterclockwise degeneracy. In the application to limaçon cavities, we investigate the evolution of mode patterns with increasing deformations, and our method works well even at relatively large deformations and is able to provide better approximations compared with the available second-order perturbation method in the literature. For the resonance, the results obtained by using our linear perturbation method are almost identical to those of the available linear perturbation methods in the literature. In the application to spiral cavities, our method accurately demonstrates mode patterns even at quasidegeneracy and the CW-CCW mode splitting phenomenon, where the perturbation methods in literature fails. Moreover, high-order perturbation solutions can also be obtained under our perturbation framework.

[1] K. J. Vahala, Nature (London) **424**, 839 (2003).
[2] S. L. McCall, A. F. J. Levi, R. E. Slusher, S. J. Pearton, and R. A. Logan, Appl. Phys. Lett. **60**, 289 (1992).
[3] K. Djordjev, S.-J. Choi, S.-J. Choi, and R. D. Dapkus, IEEE Photonics Technol. Lett. **14**, 828 (2002).
[4] L. He, Ş. K. Özdemir, J. Zhu, W. Kim, and L. Yang, Nat. Nanotechnol. **6**, 428 (2011).
[5] F. Vollmer and L. Yang, Nanophotonics **1**, 267 (2012).
[6] S. Sunada and T. Harayama, Opt. Express **15**, 16245 (2007).
[7] L. Rayleigh, Philos. Mag. **20**, 1001 (1910).
[8] G. D. Chern, H. E. Tureci, A. D. Stone, R. K. Chang, M. Kneissl, and N. M. Johnson, Appl. Phys. Lett. **83**, 1710 (2003).
[9] M. Hentschel, T.-Y. Kwon, M. A. Belkin, R. Audet, and F. Capasso, Opt. Express **17**, 10335 (2009).

[10] J. Kullig and J. Wiersig, Phys. Rev. A **94**, 043850 (2016).
[11] S.-Y. Lee, S. Rim, J.-W. Ryu, T.-Y. Kwon, M. Choi, and C.-M. Kim, Phys. Rev. Lett. **93**, 164102 (2004).
[12] J. Wiersig and M. Hentschel, Phys. Rev. Lett. **100**, 033901 (2008).
[13] C. Yan, Q. J. Wang, L. Diehl, M. Hentschel, J. Wiersig, N. Yu, C. Pflügl, F. Capasso, M. A. Belkin, T. Edamura, M. Yamanishi, and H. Kan, Appl. Phys. Lett. **94**, 251101 (2009).
[14] Q. Song, W. Fang, B. Liu, S.-T. Ho, G. S. Solomon, and H. Cao, Phys. Rev. A **80**, 041807 (2009).
[15] C.-H. Yi, M.-W. Kim, and C.-M. Kim, Appl. Phys. Lett. **95**, 141107 (2009).
[16] M. Kraft and J. Wiersig, Phys. Rev. A **89**, 023819 (2014).
[17] L. Ge, R. Sarma, and H. Cao, Optica **2**, 323 (2015).
[18] H. G. L. Schwefel, N. B. Rex, H. E. Tureci, R. K. Chang, A. D. Stone, T. Ben-Messaoud, and J. Zyss, J. Opt. Soc. Am. B **21**, 923 (2004).
[19] S. V. Boriskina, T. M. Benson, P. Sewell, and A. I. Nosich, IEEE J. Sel. Top. Quant. Electron. **12**, 52 (2006).
[20] Q. J. Wang, C. Yan, N. Yu, J. Unterhinninghofen, J. Wiersig, C. Pflügl, L. Diehl, T. Edamura, M. Yamanishi, H. Kan, and F. Capasso, Proc. Natl. Acad. Sci. U. S. A. **107**, 22407 (2010).
[21] C. P. Dettmann, G. V. Morozov, M. Sieber, and H. Waalkens, Phys. Rev. A **80**, 063813 (2009).
[22] Q. H. Song, L. Ge, J. Wiersig, J.-B. Shim, J. Unterhinninghofen, A. Eberspächer, W. Fang, G. S. Solomon, and H. Cao, Phys. Rev. A **84**, 063843 (2011).
[23] S. F. Liew, B. Redding, L. Ge, G. S. Solomon, and H. Cao, Appl. Phys. Lett. **104**, 231108 (2014).
[24] J. Wiersig and M. Hentschel, Phys. Rev. A **73**, 031802 (2006).
[25] M. Kraft and J. Wiersig, Phys. Rev. A **94**, 013851 (2016).
[26] J. U. Nöckel and A. D. Stone, Nature (London) **385**, 45 (1997).
[27] N. B. Rex, H. E. Tureci, H. G. L. Schwefel, R. K. Chang, and A. D. Stone, Phys. Rev. Lett. **88**, 094102 (2002).
[28] Q. H. Song, L. Ge, A. D. Stone, H. Cao, J. Wiersig, J.-B. Shim, J. Unterhinninghofen, W. Fang, and G. S. Solomon, Phys. Rev. Lett. **105**, 103902 (2010).
[29] H. Cao and J. Wiersig, Rev. Mod. Phys. **87**, 61 (2015).
[30] C. M. Bender, Rep. Prog. Phys. **70**, 947 (2007).
[31] M. Brandstetter, M. Liertzer, C. Deutsch, P. Klang, J. Schöberl, H. E. Türeci, G. Strasser, K. Unterrainer, and S. Rotter, Nat. Commun. **5**, 4034 (2014).
[32] B. Peng, Ş. K. Özdemir, S. Rotter, H. Yilmaz, M. Liertzer, F. Monifi, C. M. Bender, F. Nori, and L. Yang, Science **346**, 328 (2014).
[33] R. Dubertrand, E. Bogomolny, N. Djellali, M. Lebental, and C. Schmit, Phys. Rev. A **77**, 013804 (2008).
[34] L. Ge, Q. Song, B. Redding, and H. Cao, Phys. Rev. A **87**, 023833 (2013).
[35] J. D. Jackson, *Classical Electrodynamics*, 3rd ed. (Wiley, New York, 1999).
[36] D. Colton and R. Kress, *Inverse Acoustic and Electromagnetic Scattering Theory* (Springer, New York, 2013).
[37] C.-H. Yi, J. Kullig, and J. Wiersig, Phys. Rev. Lett. **120**, 093902 (2018).
[38] J. Wiersig, A. Eberspächer, J.-B. Shim, J.-W. Ryu, S. Shinohara, M. Hentschel, and H. Schomerus, Phys. Rev. A **84**, 023845 (2011).
[39] J. Wiersig, S. W. Kim, and M. Hentschel, Phys. Rev. A **78**, 053809 (2008).
[40] B. Redding, L. Ge, Q. Song, J. Wiersig, G. S. Solomon, and H. Cao, Phys. Rev. Lett. **108**, 253902 (2012).
[41] W. D. Heiss, J. Phys. A: Math. Theor. **41**, 244010 (2008).